Article

Free Energy Surfaces and Barriers for Vacancy Diffusion on Al(100), Al(110), Al(111) Reconstructed Surfaces

Junais Habeeb Mokkath [1,*], Mufasila Mumthaz Muhammed [2] and Ali J. Chamkha [3]

[1] Quantum Nanophotonics Simulations Lab, Department of Physics, Kuwait College of Science and Technology, Doha Area, 7th Ring Road, Kuwait City P.O. Box 27235, Kuwait

[2] School of Engineering & Computing, American International University, Saad Al Abdullah-East of Naseem, Block 3, Kuwait; m.muhammed@aiu.edu.kw

[3] Faculty of Engineering, Kuwait College of Science and Technology, Doha 35004, Kuwait; a.chamkha@kcst.edu.kw

* Correspondence: j.mokath@kcst.edu.kw

Abstract: Metadynamics is a popular enhanced sampling method based on the recurrent application of a history-dependent adaptive bias potential that is a function of a selected number of appropriately chosen collective variables. In this work, using metadynamics simulations, we performed a computational study for the diffusion of vacancies on three different Al surfaces [reconstructed Al(100), Al(110), and Al(111) surfaces]. We explored the free energy landscape of diffusion and estimated the barriers associated with this process on each surface. It is found that the surfaces are unique regarding vacancy diffusion. More specially, the reconstructed Al(110) surface presents four metastable states on the free energy surface having sizable and connected passage-ways with an energy barrier of height 0.55 eV. On the other hand, the reconstructed Al(100)/Al(111) surfaces exhibit two/three metastable states, respectively, with an energy barrier of height 0.33 eV. The findings in this study can help to understand surface vacancy diffusion in technologically relevant Al surfaces.

1. Introduction

Molecular dynamics (MD) simulations have been shown to be an indispensable toolkit for efficient exploration of the configurational space of complex systems, since they render dynamical evolution with in-depth atomistic level details. Notwithstanding recent advancements in purpose-built computational resources and software tools, the timescales of milliseconds and beyond remains a longstanding (inherent) problem for MD simulations [1,2]. Consequentially, the possibility of understanding longtime scale phenomena like "rare events" (more specifically, an event happening at low frequency such as protein folding and nucleation) is still beyond the reach of MD simulations. To overcome this limitation, significant effort has been devoted to developing a great variety of enhanced sampling methods [3–17]. Metadynamics (MetaD) [18–28] is one such well-established enhanced sampling method which has been successfully applied to a variety of areas in biophysics and material science, to list a few. The power of MetaD simulation is its simplicity: it captures rare events and maps out the underlying free energy surface. MetaD utilizes the recurrent application of a history dependent adaptive bias potential (that helps to locate regions in the configurational space separated by high energy barriers and enhance minima-to-minima transitions) to a limited number of degrees of freedom called collective variables (CVs) [29–33]. Over the last few years, a multitude of CVs have been employed including coordination numbers, lattice parameters, interatomic angles, and potential energy, to mention a few. More specifically, CVs provide a low-dimensional projection of the configurational space and are selected to describe modes of the system

that are more difficult to explore. Also, note that the different metastable states of a system should correspond to different values of the CVs.

In this work, we employ MetaD simulations to study the free energy surfaces and free energy barriers of low-index Al(100), Al(110), and Al(111) systems having a surface vacancy. Al is of particular interest recently due to its exceptional properties [34–39]. On the other hand, defects like vacancy are omnipresent on crystals and play an important role in their properties [40–44]. Substantial experimental and theoretical efforts have been employed over many years to elucidate the free energy surfaces and free energy barriers of diffusion on crystal surfaces [45–48]. How diffusion happens on the atomic scale on a crystal surface is a fundamental problem, and a detailed knowledge of the diffusion process is crucial for applications that demand high technological precision [49–51]. Importantly, vacancy diffusion is a thermally activated process demanding the system to overcome free energy barriers. Generally, free energy barriers are higher than thermal energy, and therefore, the diffusion process is regarded as a rare event.

A detailed understanding of free energy surfaces and free energy barriers are essential cornerstones for the design and fabrication of nanodevices with enhanced performance. While experiments face challenges in identifying and characterizing diffusion processes, simulation approaches can predict them accurately. To our knowledge, vacancy diffusion on reconstructed Al surfaces has not been investigated yet by MetaD simulations. Our paper aims at filling this gap. The remainder of this paper is organized as follows. In the following section, we provide the details of the computational methodology we used. Next, we discuss the important results from our simulations, such as the radial distribution functions, mass density profiles, two-dimensional free energy surfaces, and free energy barriers on the reconstructed Al(100), Al(110), and Al(111) surfaces. As a key result in this study, the highest barrier for vacancy diffusion is found in the case of Al(110) surface due to its more open nature. The results obtained in this work would help in a better understanding of the modulations in the vacancy diffusion process on different low-index Al surfaces, beneficial for Al based technology.

2. System and Computational Aspects

MetaD simulations were carried out using a standard protocol by the PLUMED software version 2.1 [52] interfaced to the QuantumWise Atomistix ToolKit (QuantumATK) software package [53]. This plugin provides customized software libraries for a variety of CVs and also renders several post-processing tools. Our MetaD simulations involve several steps: (a) modeling of Al(100), Al(110), Al(111) surfaces and definition of Al-Al atomic interaction; (b) governing equations for the system, conditions of simulation and energy minimization; and (c) integration scheme and calculation of concerned properties. Now, regarding the systems under investigation, we created low-index Al(100), Al(110), Al(111) slabs with 4×4 surface lattice from the bulk Al. Each of these slabs is composed of six layers with a total number of 96 atoms. Nevertheless, the slab thickness is different from each other. The Al-Al atomic interactions were described using the EAM (embedded atom method) potential [54]. Briefly, the EAM potential can be written as: $E_{\text{tot}} = \frac{1}{2} \sum_{i \neq j} V(r_{ij}) + \sum_i F(\rho_i)$ with $\rho_i = \sum_j \phi(r_{ij})$ where E_{tot} is the total energy, $V(r_{ij})$ the pair potential, $F(\rho_i)$ the embedding function, and $\phi(r_{ij})$ the electron density contribution from atom j to atom i. The total electron density ρ_i at an atom position i is calculated via the linear superposition of electron density contributions from neighboring atoms. For each MetaD simulation run, a single Al surface vacancy was generated by removing the atom of the topmost layer with position $x = 0$ and $y = 0$. In the next step, we performed structure optimization. In all slabs, we allowed the atoms occupying two top most layers to relax, while the atomic positions of those atoms occupying the four bottom layers were kept fixed to mimic bulk constraints; see Figure 1. To avoid the spurious interaction between the slab and its periodic images, a vacuum distance of 15 Å used along the perpendicular direction to the slab.

Reconstructed Al surfaces having a surface vacancy
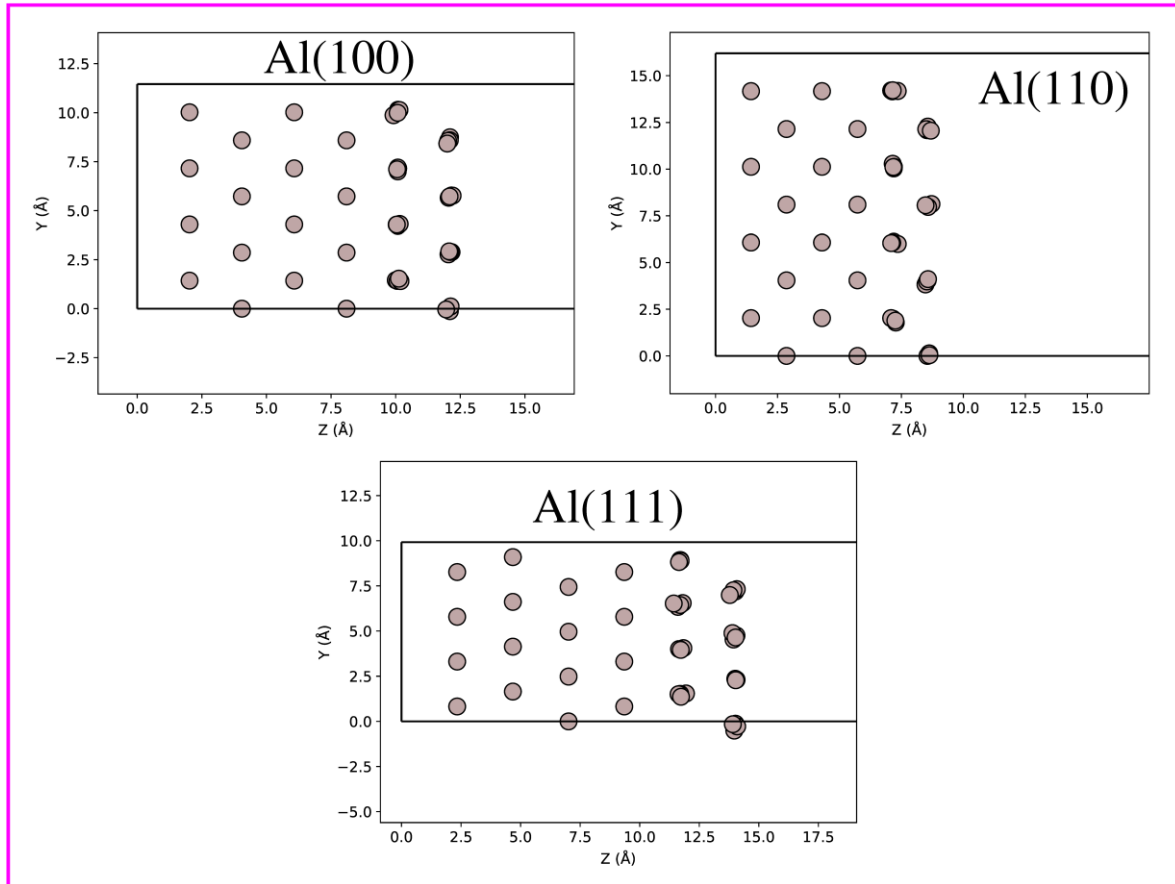
Figure 1. Reconstructed Al(100), Al(110), Al(111) slabs having a surface vacancy. Note that the atoms in the two top most layers were allowed to relax while the atoms occupying the four bottom layers were fixed.

Each simulation run was force-minimized and then equilibrated for 10,000,000 timesteps using Langevin method [55,56]. Since the starting Al(100), Al(110), and Al(111) slab structures will relax because of the vacancy creation, MetaD was started only after 10,000 time steps, which was sufficient for relaxation. We have chosen two CVs defined by distance traveled by the atom p (an atom on the surface just next to the vacancy) along the Cartesian axes, x and y (with no bias in the direction or pathway of migration). Minima-to-minima transitions were made possible within the simulation timescale via a history-dependent bias potential [52] (applied to all atoms in the two top most layers) constructed by summing Gaussian contributions of height h and width w in the space defined by the CV as follows:

$$\Delta V(\eta) = \sum_{k<nG} w_k \exp\left[\frac{(\eta - \eta(k\tau G))}{2\delta^2}\right] \tag{1}$$

where $\Delta V(\eta)$ is the history-dependent bias potential, η is the CV used, τ is the Gaussian deposition stride, w and δ are the Gaussian height and width, respectively. The $\Delta V(\eta)$ is updated, and while the simulation runs, it fills the underlying free energy surface helping the crossing of the energy barriers. We remark that several test runs were first performed to optimize the various simulation parameters such as the height and width of the Gaussians. We choose $w = 0.05$ eV and $\delta = 0.025$ eV considering the accuracy and CPU time. Gaussians were deposited every 1000 time-steps. It should be stressed that $\Delta V(_\eta)$ bias encourages the sampling of the unfavorable states by kicking the system out of the most favorable ones.

3. Results and Discussion

Before we begin our analysis and discussion on the free energy surfaces and free energy barriers of low-index Al(100), Al(110), Al(111) surfaces, it is informative to provide first the results of the structure optimizations, see Figure 1. In this context, we provide the radial distribution functions (RDFs) and mass density profiles of the reconstructed Al(100), Al(110), Al(111) surfaces, see Figure 2. We have calculated the RDFs (see the left panel of Figure 2) using the equation $g(r) = \frac{1}{4\pi r^2} \frac{1}{N\rho} \sum_{i=1}^{N} \sum_{j \neq i}^{N} \langle \delta(r - |r_i - r_j|) \rangle$. As common to all the investigated systems, the RDFs show a pronounced peak at around 2.875 Å, indicating that this is the dominant nearest-neighbor distance between Al atoms. This value is very close to the nearest-neighbor distance between Al atoms in crystalline Al (2.856 Å) at room temperature [57]. Next, we analyse the mass density profiles, see the right panel of Figure 2. It shows how mass is distributed along the perpendicular direction to the slab. One easily concludes that mass density profiles are markedly different from each other due to the unique distributions of Al atoms in the Al(100), Al(110), and Al(111) configurations. Additionally, small modulations to the mass density profiles are also contributed by atom displacements during structure optimization. It is noteworthy that Al(100), Al(110), and Al(111) mass density profiles plummeted to zero at around 15.10 Å, 11.50 Å, and 17.20 Å, respectively. This result is in agreement with the fact that Al(110) slab is more compact and open in comparison to the Al(100) and Al(111) slabs, see Figure 1. It is also important to emphasize that an inward relaxation of the top layer is observed in all reconstructed structures, see Figure 1. This arises due to the surface asymmetry, where the force of attraction will be greater for bulk atoms causing a significant inward relaxation of the top surface layer [58].

After having analysed and discussed the structural features of the reconstructed Al(100), Al(110), Al(111) slabs having a surface vacancy, next we investigate the free energy surfaces [F(s)] as a function of the CV1 and CV2, see the left panel in Figure 3. The plots show a heat map of F(s) as a function of the chosen CVs. It is noteworthy that F(s) corresponding to Al(100), Al(110) and Al(111) structures yield unique and interesting features as being composed of different metastable states. More specifically, in the case of Al(100) slab, one finds four basins or metastable states on the free energy surface (see the top left panel in Figure 3), corresponding to the diffusion of the vacancy from one site to the neighboring one. Interestingly, one observes that the three metastable states are well connected by sizable passageways. It is important to mention that metastable states that are connected by passageways allow rare but crucial transitions from one state to another. Additionally, it is noteworthy that with chosen CV1 and CV2, the F(s) clearly separate the metastable states. In the case of Al(100) structure, one finds that CV1 can distinguish the four different metastable states, while CV2 is not. Technically speaking, metastability originates when the probability distribution as a function of the atomic coordinates has at least two peaks separated by a region in which the probability is many orders of magnitude lower. The metastable states displayed in Figure 3 are akin to an archetypal example in which a molecule that can undergo a chemical reaction [59]. In the case of A(110) and Al(111) slabs, one finds two and three metastable states on the free energy surface, respectively. More specifically, in the case of Al(110) slab, the two metastable states are connected by a narrow passageway and CV1 is crucial than CV2 since the former clearly separates the two available metastable states. The free energy surface of Al(111) is more interesting. One finds that metastable states are positioned more or less on the corners of a triangle with no passageway on one side. On the other hand, CV1 again appears to be the best performing CV, nonetheless, CV2 can also be helpful in identifying at least two metastable states on the free energy surface.
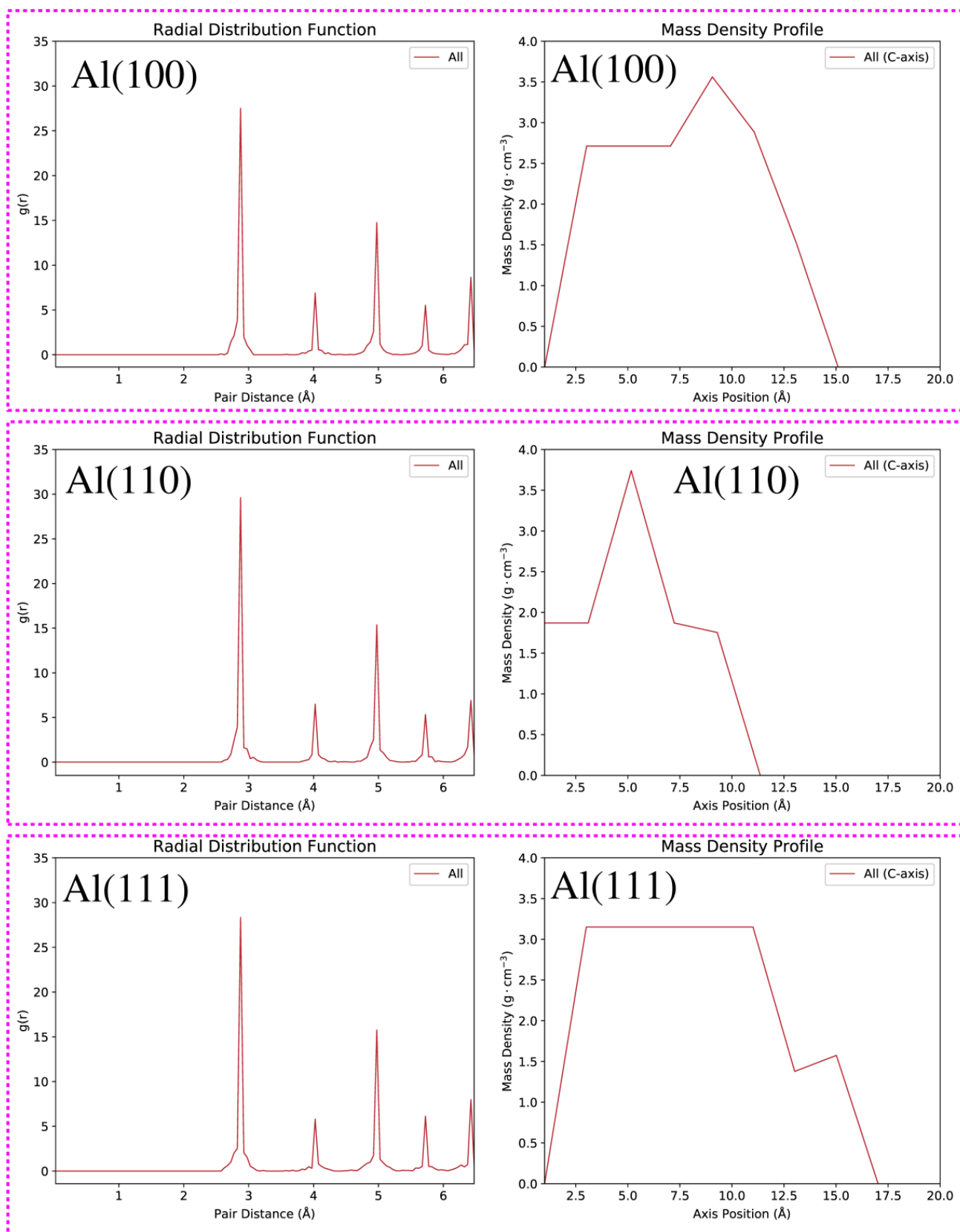
Figure 2. RDFs (**left** panel) and mass density profiles (**right** panel) of the reconstructed Al(100), Al(110), Al(111) slabs having a surface vacancy.
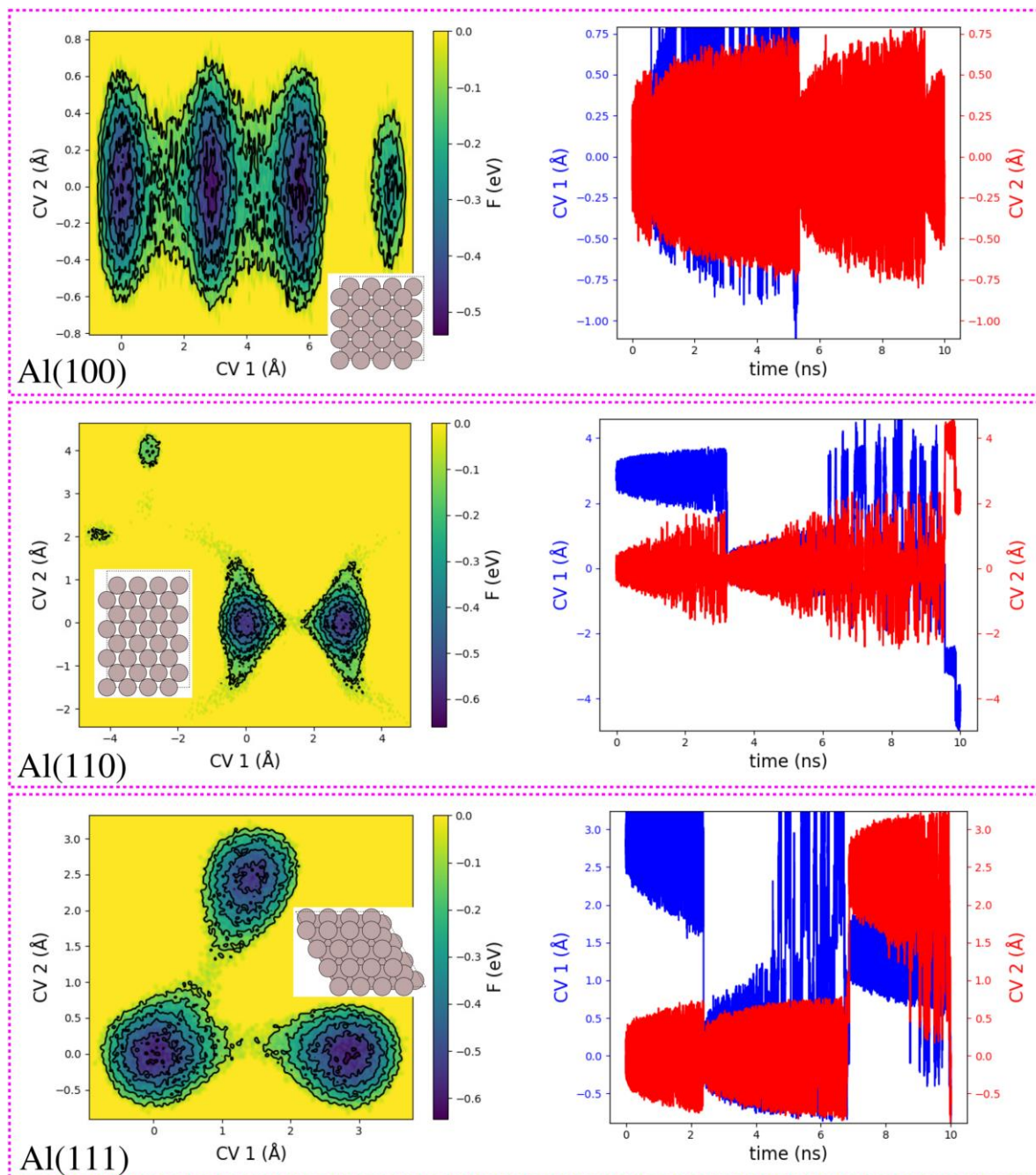
Figure 3. Plots showing the free energy surfaces as a function of the chosen CVs (**left** panel) and evolution of the CVs over the simulation time in nanoseconds (**right** panel) of the reconstructed Al(100), Al(110), and Al(111) slabs having a surface atomic vacancy. All energy values are in eV and all distance values are in Å.

It is also interesting to analyse how the collective variables, CV1 and CV2 evolve over simulation time, see the right panel of Figure 3. More specifically, in the case of Al(100) slab, one finds that CV2, which corresponds to the y Cartesian coordinate, oscillates around a constant value of 0 Å. This is because all the three (connected) metastable states appear at the same y value. The first, second, and third metastable states are filled until at approximately 5.20 ns, 9.50 ns, and 10.10 ns, respectively. In contrast, the evolution of CV1, which corresponds to the x Cartesian coordinate, suggests that it is filled until at approximately 5.20 ns. Now let us move onto Al(110) slab. One finds that CV2, which corresponds to the y Cartesian coordinate, oscillates around a constant value of 0 Å, because

both the metastable states occur at the same y position. One finds that both CV1 and CV2 are filled at approximately 3.20 ns. Finally, in the case of Al(111), CV2 is filled at approximately 2.30 ns and 6.80 ns. However, in the case of CV1, it is filled at approximately 2.30 ns. Then it goes to the second metastable state oscillating around 0 Å and jump to the third metastable state oscillating around 1.50 Å.

Having analysed and discussed the free energy surfaces and evolution of CVs over simulation time in detail, it is worthwhile to estimate the free energy barrier for surface vacancy diffusion at low-index Al(100), Al(110), Al(111) surfaces, see Figure 4. One finds that the free energy barrier of Al(100) and Al(111) slabs amount to 0.33 eV (thus energetically very similar), while the free energy barrier of Al(110) amounts to a higher value of 0.55 eV. These results are in relatively good agreement with the previous work reporting vacancy diffusion on the different Al surfaces [28]. Vacancy diffusion at the Al(110) surface has twice the barrier as Al(100) and Al(111) surfaces is highly likely due to the open nature of the Al(110) surface. As expected, on an open surface, vacancy diffusion finds it more difficult since it has to overcome large energy barriers. These results are in tune with the previous MetaD study (Cu surfaces) finding that there are strong differences in the mobilities of the vacancies depending on the specific surface [60]. Finally, it is worthwhile to mention that ref. [28] reported two energy barriers for adatom diffusion on Al(110) surface; one parallel to the surface and other perpendicular to the surface. Nevertheless, in the present study, we found a single energy barrier for vacancy diffusion on Al(110) surface. This is due to differences in the diffusion process.
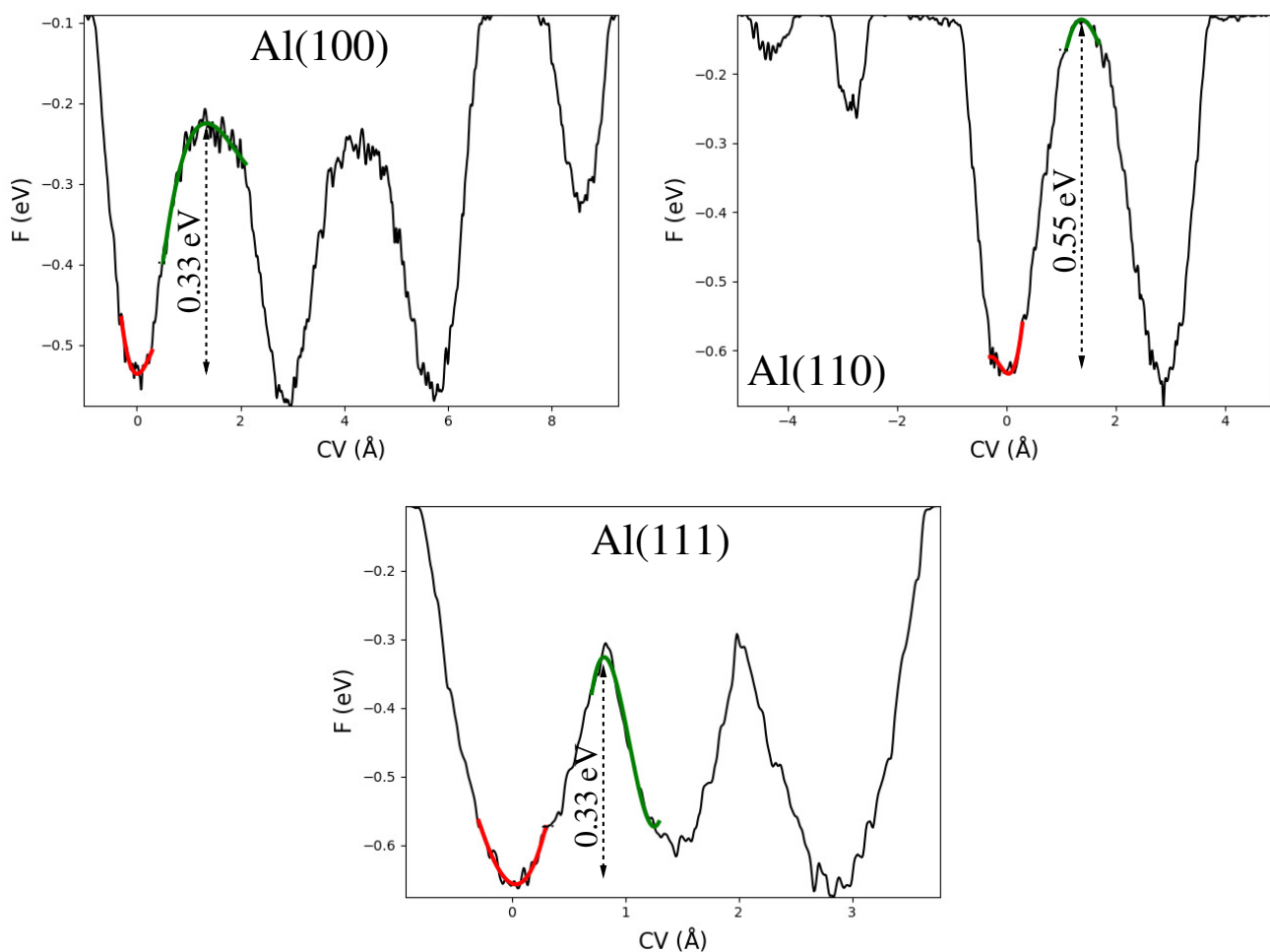
Figure 4. The free energy barriers on the reconstructed Al(100), Al(110), and Al(111) slabs having a surface vacancy. All energy values are in eV and all distance values are in Å.

4. Summary and Outlook

Exploring and quantifying free energy surfaces (FESs) is the key to the comprehension of a plethora of phenomena in chemistry, materials science, and biophysics. Generally, FESs are characterized by several metastable states separated by large free energy barriers. To overcome these barriers and efficiently sample configurational space, it is worthwhile to employ enhanced sampling techniques such as MetaD simulations. Here, we have presented a detailed study elucidating the free energy surfaces and free energy barriers for surface vacancy diffusion on low-index Al surfaces using MetaD simulations. With the use of these exemplary reconstructed surfaces, we reveal the unique vacancy diffusion process. The reconstructed Al(110) surface presents four metastable states on the FES. Among them, three metastable states are well connected by sizable passageways leading to rare but crucial transitions. On the other hand, the reconstructed Al(110) structure presents two metastable states that are connected by a narrow passageway and the reconstructed Al(111) surface presents three metastable states that are positioned on the three corners of a triangle. The results in this study will help to understand Al surfaces with vacancy defects which are necessary to design highly efficient Al based devices. While here we have restricted our work to Al vacancy diffusion, this work can be considered as a step toward the general structural and dynamical characterization of other types of defects.

Author Contributions: Conceptualization, J.H.M.; methodology, J.H.M.; software, J.H.M.; validation, J.H.M.; M.M.M. and A.J.C.; formal analysis, J.H.M.; investigation, J.H.M.; resources, J.H.M.; data curation, J.H.M.; writing—original draft preparation, J.H.M.; writing—review and editing, J.H.M. and M.M.M.; visualization, J.H.M.; supervision, A.J.C.; project administration, J.H.M.; funding acquisition, J.H.M. All authors have read and agreed to the published version of the manuscript.

Institutional Review Board Statement: Not applicable.

Informed Consent Statement: Not applicable.

Data Availability Statement: The data presented in this study are available on request from the corresponding author.

Conflicts of Interest: The authors declare no conflict of interest.

Nomenclature

Å	Angstrom
CV	Collective variable
EAM	Embedded atom method
F(s)	Free energy surface
MetaD	Metadynamic
ns	Nanosecond
RDF	Radial distribution function

References

1. Lindorff-Larsen, K.; Piana, S.; Dror, R.O.; Shaw, D.E. How Fast-Folding Proteins Fold. *Science* **2011**, *334*, 517–520. [CrossRef] [PubMed]
2. Tiwary, P.; Limongelli, V.; Salvalaglio, M.; Parrinello, M. Kinetics of protein–ligand unbinding: Predicting pathways, rates, and rate-limiting steps. *Proc. Natl. Acad. Sci. USA* **2015**, *112*, E386–E391. [CrossRef]
3. Torrie, G.; Valleau, J. Nonphysical sampling distributions in Monte Carlo free-energy estimation: Umbrella sampling. *J. Comput. Phys.* **1977**, *23*, 187–199. [CrossRef]
4. Grubmüller, H. Predicting slow structural transitions in macromolecular systems: Conformational flooding. *Phys. Rev. E* **1995**, *52*, 2893–2906. [CrossRef] [PubMed]
5. Sprik, M.; Ciccotti, G. Free energy from constrained molecular dynamics. *J. Chem. Phys.* **1998**, *109*, 7737–7744. [CrossRef]
6. Voter, A.F. A method for accelerating the molecular dynamics simulation of infrequent events. *J. Chem. Phys.* **1997**, *106*, 4665–4677. [CrossRef]

7. Steiner, M.M.; Genilloud, P.A.; Wilkins, J.W. Simple bias potential for boosting molecular dynamics with the hyperdynamics scheme. *Phys. Rev. B* **1998**, *57*, 10236–10239. [CrossRef]

8. VandeVondele, J.; Rothlisberger, U. Efficient multidimensional free energy calculations for ab initio molecular dynamics using classical bias potentials. *J. Chem. Phys.* **2000**, *113*, 4863–4868. [CrossRef]

9. Rahman, J.A.; Tully, J.C. Puddle-skimming: An efficient sampling of multidimensional configuration space. *J. Chem. Phys.* **2002**, *116*, 8750–8760. [CrossRef]

10. Mezei, M. Adaptive umbrella sampling: Self-consistent determination of the non-Boltzmann bias. *J. Comput. Phys.* **1987**, *68*, 237–248. [CrossRef]

11. Henkelman, G.; Uberuaga, B.P.; Jónsson, H. A climbing image nudged elastic band method for finding saddle points and minimum energy paths. *J. Chem. Phys.* **2000**, *113*, 9901–9904. [CrossRef]

12. El-Mellouhi, F.; Mousseau, N.; Lewis, L.J. Kinetic activation-relaxation technique: An off-lattice self-learning kinetic Monte Carlo algorithm. *Phys. Rev. B* **2008**, *78*, 153202. [CrossRef]

13. Mees, M.J.; Pourtois, G.; Neyts, E.C.; Thijsse, B.J.; Stesmans, A. Uniform-acceptance force-bias Monte Carlo method with time scale to study solid-state diffusion. *Phys. Rev. B* **2012**, *85*, 134301. [CrossRef]

14. Wang, Y.; Valsson, O.; Tiwary, P.; Parrinello, M.; Lindorff-Larsen, K. Frequency adaptive metadynamics for the calculation of rare-event kinetics. *J. Chem. Phys.* **2018**, *149*, 072309. [CrossRef]

15. Debnath, J.; Parrinello, M. Gaussian Mixture-Based Enhanced Sampling for Statics and Dynamics. *J. Phys. Chem. Lett.* **2020**, *11*, 5076–5080. [CrossRef]

16. Bartels, C.; Karplus, M. Probability Distributions for Complex Systems: Adaptive Umbrella Sampling of the Potential Energy. *J. Phys. Chem. B* **1998**, *102*, 865–880. [CrossRef]

17. Maragliano, L.; Vanden-Eijnden, E. A temperature accelerated method for sampling free energy and determining reaction pathways in rare events simulations. *Chem. Phys. Lett.* **2006**, *426*, 168–175. [CrossRef]

18. Laio, A.; Parrinello, M. Escaping free-energy minima. *Proc. Natl. Acad. Sci. USA* **2002**, *99*, 12562–12566. [CrossRef]

19. Barducci, A.; Bonomi, M.; Parrinello, M. Metadynamics. *WIREs Comput. Mol. Sci.* **2011**, *1*, 826–843. [CrossRef]

20. Sutto, L.; Marsili, S.; Gervasio, F.L. New advances in metadynamics. *WIREs Comput. Mol. Sci.* **2012**, *2*, 771–779. [CrossRef]

21. Valsson, O.; Tiwary, P.; Parrinello, M. Enhancing Important Fluctuations: Rare Events and Metadynamics from a Conceptual Viewpoint. *Annu. Rev. Phys. Chem.* **2016**, *67*, 159–184. [CrossRef] [PubMed]

22. Bussi, G.; Laio, A.; Parrinello, M. Equilibrium Free Energies from Nonequilibrium Metadynamics. *Phys. Rev. Lett.* **2006**, *96*, 090601. [CrossRef] [PubMed]

23. Barducci, A.; Bussi, G.; Parrinello, M. Well-Tempered Metadynamics: A Smoothly Converging and Tunable Free-Energy Method. *Phys. Rev. Lett.* **2008**, *100*, 020603. [CrossRef] [PubMed]

24. Pfaendtner, J.; Bonomi, M. Efficient Sampling of High-Dimensional Free-Energy Landscapes with Parallel Bias Metadynamics. *J. Chem. Theory Comput.* **2015**, *11*, 5062–5067. [CrossRef] [PubMed]

25. Branduardi, D.; Bussi, G.; Parrinello, M. Metadynamics with Adaptive Gaussians. *J. Chem. Theory Comput.* **2012**, *8*, 2247–2254. [CrossRef]

26. Casasnovas, R.; Limongelli, V.; Tiwary, P.; Carloni, P.; Parrinello, M. Unbinding Kinetics of a p38 MAP Kinase Type II Inhibitor from Metadynamics Simulations. *J. Am. Chem. Soc.* **2017**, *139*, 4780–4788. [CrossRef]

27. Dama, J.F.; Rotskoff, G.; Parrinello, M.; Voth, G.A. Transition-Tempered Metadynamics: Robust, Convergent Metadynamics via On-the-Fly Transition Barrier Estimation. *J. Chem. Theory Comput.* **2014**, *10*, 3626–3633. [CrossRef]

28. Stumpf, R.; Scheffler, M. Ab initio calculations of energies and self-diffusion on flat and stepped surfaces of Al and their implications on crystal growth. *Phys. Rev. B* **1996**, *53*, 4958–4973. [CrossRef]

29. Chen, W.; Ferguson, A.L. Molecular enhanced sampling with autoencoders: On-the-fly collective variable discovery and accelerated free energy landscape exploration. *J. Comput. Chem.* **2018**, *39*, 2079–2102. [CrossRef]

30. Fiorin, G.; Klein, M.L.; Hénin, J. Using collective variables to drive molecular dynamics simulations. *Mol. Phys.* **2013**, *111*, 3345–3362. [CrossRef]

31. Bonati, L.; Rizzi, V.; Parrinello, M. Data-Driven Collective Variables for Enhanced Sampling. *J. Phys. Chem. Lett.* **2020**, *11*, 2998–3004. [CrossRef] [PubMed]

32. Mendels, D.; Piccini, G.; Parrinello, M. Collective Variables from Local Fluctuations. *J. Phys. Chem. Lett.* **2018**, *9*, 2776–2781. [CrossRef] [PubMed]

33. Brotzakis, Z.F.; Limongelli, V.; Parrinello, M. Accelerating the Calculation of Protein–Ligand Binding Free Energy and Residence Times Using Dynamically Optimized Collective Variables. *J. Chem. Theory Comput.* **2019**, *15*, 743–750. [CrossRef] [PubMed]

34. Zhou, L.; Zhang, C.; McClain, M.J.; Manjavacas, A.; Krauter, C.M.; Tian, S.; Berg, F.; Everitt, H.O.; Carter, E.A.; Nordlander, P.; et al. Aluminum Nanocrystals as a Plasmonic Photocatalyst for Hydrogen Dissociation. *Nano Lett.* **2016**, *16*, 1478–1484. [CrossRef]

35. Swearer, D.F.; Robatjazi, H.; Martirez, J.M.P.; Zhang, M.; Zhou, L.; Carter, E.A.; Nordlander, P.; Halas, N.J. Plasmonic Photocatalysis of Nitrous Oxide into N_2 and O_2 Using Aluminum–Iridium Antenna–Reactor Nanoparticles. *ACS Nano* **2019**, *13*, 8076–8086. [CrossRef]

36. Chen, Y.; Xin, X.; Zhang, N.; Xu, Y.J. Aluminum-Based Plasmonic Photocatalysis. *Part. Part. Syst. Charact.* **2017**, *34*, 1600357. [CrossRef]

37. Yuan, L.; Lou, M.; Clark, B.D.; Lou, M.; Zhou, L.; Tian, S.; Jacobson, C.R.; Nordlander, P.; Halas, N.J. Morphology-Dependent Reactivity of a Plasmonic Photocatalyst. *ACS Nano* **2020**, *14*, 12054–12063. [CrossRef]

38. Robatjazi, H.; Lou, M.; Clark, B.D.; Jacobson, C.R.; Swearer, D.F.; Nordlander, P.; Halas, N.J. Site-Selective Nanoreactor Deposition on Photocatalytic Al Nanocubes. *Nano Lett.* **2020**, *20*, 4550–4557. [CrossRef]

39. Renard, D.; Tian, S.; Ahmadivand, A.; DeSantis, C.J.; Clark, B.D.; Nordlander, P.; Halas, N.J. Polydopamine-Stabilized Aluminum Nanocrystals: Aqueous Stability and Benzo[a]pyrene Detection. *ACS Nano* **2019**, *13*, 3117–3124. [CrossRef]

40. Schwoebel, R.L.; Shipsey, E.J. Step Motion on Crystal Surfaces. *J. Appl. Phys.* **1966**, *37*, 3682–3686. [CrossRef]

41. Mahmoud, S.; Carrez, P.; Landeiro Dos Reis, M.; Mousseau, N.; Cordier, P. Diffusion mechanism of bound Schottky defect in magnesium oxide. *Phys. Rev. Mater.* **2021**, *5*, 033609. [CrossRef]

42. Zheng, J.; Ju, Z.; Zhang, B.; Nai, J.; Liu, T.; Liu, Y.; Xie, Q.; Zhang, W.; Wang, Y.; Tao, X. Lithium ion diffusion mechanism on the inorganic components of the solid–electrolyte interphase. *J. Mater. Chem. A* **2021**, *9*, 10251–10259. [CrossRef]

43. Šimonová Baranyaiová, T.; Mészáros, R.; Sebechlebská, T.; Bujdák, J. Non-Arrhenius kinetics and slowed-diffusion mechanism of molecular aggregation of a rhodamine dye on colloidal particles. *Phys. Chem. Chem. Phys.* **2021**, *23*, 17177–17185. [CrossRef] [PubMed]

44. Sadowski, M.; Albe, K. Influence of Br^-/S^{2-} site-exchange on Li diffusion mechanism in Li_6PS_5Br: A computational study. *Philos. Trans. R. Soc. A Math. Phys. Eng. Sci.* **2021**, *379*, 20190458. [CrossRef] [PubMed]

45. McCarty, K.F.; Nobel, J.A.; Bartelt, N.C. Vacancies in solids and the stability of surface morphology. *Nature* **2001**, *412*, 622–625. [CrossRef] [PubMed]

46. Cowern, N.E.B.; Simdyankin, S.; Ahn, C.; Bennett, N.S.; Goss, J.P.; Hartmann, J.M.; Pakfar, A.; Hamm, S.; Valentin, J.; Napolitani, E.; et al. Extended Point Defects in Crystalline Materials: Ge and Si. *Phys. Rev. Lett.* **2013**, *110*, 155501. [CrossRef]

47. Südkamp, T.; Bracht, H. Self-diffusion in crystalline silicon: A single diffusion activation enthalpy down to 755 °C. *Phys. Rev. B* **2016**, *94*, 125208. [CrossRef]

48. Ishikawa, R.; Mishra, R.; Lupini, A.R.; Findlay, S.D.; Taniguchi, T.; Pantelides, S.T.; Pennycook, S.J. Direct Observation of Dopant Atom Diffusion in a Bulk Semiconductor Crystal Enhanced by a Large Size Mismatch. *Phys. Rev. Lett.* **2014**, *113*, 155501. [CrossRef]

49. Xiong, G.; Clark, J.N.; Nicklin, C.; Rawle, J.; Robinson, I.K. Atomic Diffusion within Individual Gold Nanocrystal. *Sci. Rep.* **2014**, *4*, 6765. [CrossRef]

50. Windl, W.; Bunea, M.M.; Stumpf, R.; Dunham, S.T.; Masquelier, M.P. First-Principles Study of Boron Diffusion in Silicon. *Phys. Rev. Lett.* **1999**, *83*, 4345–4348. [CrossRef]

51. Dolan, M.D.; McLennan, K.G.; Way, J.D. Diffusion of Atomic Hydrogen through V–Ni Alloy Membranes under Nondilute Conditions. *J. Phys. Chem. C* **2012**, *116*, 1512–1518. [CrossRef]

52. Tribello, G.A.; Bonomi, M.; Branduardi, D.; Camilloni, C.; Bussi, G. PLUMED 2: New feathers for an old bird. *Comput. Phys. Commun.* **2014**, *185*, 604–613. [CrossRef]

53. Smidstrup, S.; Markussen, T.; Vancraeyveld, P.; Wellendorff, J.; Schneider, J.; Gunst, T.; Verstichel, B.; Stradi, D.; Khomyakov, P.A.; Vej-Hansen, U.G.; et al. QuantumATK: An integrated platform of electronic and atomic-scale modelling tools. *J. Phys. Condens. Matter* **2020**, *32*, 015901. [CrossRef]

54. Winey, J.M.; Kubota, A.; Gupta, Y.M. A thermodynamic approach to determine accurate potentials for molecular dynamics simulations: Thermoelastic response of aluminum. *Model. Simul. Mater. Sci. Eng.* **2009**, *17*, 055004. [CrossRef]

55. Chandrasekhar, S. Stochastic Problems in Physics and Astronomy. *Rev. Mod. Phys.* **1943**, *15*, 1–89. [CrossRef]

56. van Gunsteren, W.; Berendsen, H. Algorithms for brownian dynamics. *Mol. Phys.* **1982**, *45*, 637–647. [CrossRef]

57. Cooper, A. Precise lattice constsants of germanium, aluminum, gallium arsenide, uranium, sulphur, quartz and sapphire. *Acta Crystallogr.* **1962**, *15*, 578–582. [CrossRef]

58. Finnis, M.W.; Heine, V. Theory of lattice contraction at aluminium surfaces. *J. Phys. F Met. Phys.* **1974**, *4*, L37–L41. [CrossRef]

59. Ensing, B.; De Vivo, M.; Liu, Z.; Moore, P.; Klein, M.L. Metadynamics as a Tool for Exploring Free Energy Landscapes of Chemical Reactions. *Accounts Chem. Res.* **2006**, *39*, 73–81. [CrossRef]

60. Kondati Natarajan, S.; Behler, J. Self-Diffusion of Surface Defects at Copper–Water Interfaces. *J. Phys. Chem. C* **2017**, *121*, 4368–4383. [CrossRef]